Orbital magnetic moments in pure and doped carbon nanotubes

Magdalena Margańska,* Marek Szopa, and Elżbieta Zipper
Department of Theoretical Physics, University of Silesia, ul Uniwersytecka 4, 40 007 Katowice, Poland
(Received 8 February 2005; revised manuscript received 21 June 2005; published 6 September 2005)

The unusual band structure of carbon nanotubes (CNs) results in their remarkable magnetic properties. The application of magnetic field **B** parallel to the tube axis can change the conducting properties of the CN from metallic to semiconducting and vice versa. Apart from that, B induces (via the Bohm-Aharonov effect) orbital magnetic moments μ_{orb} in the nanotube. These moments are studied both in pure and hole- or electron-doped CNs, isolated or in a circuit. Remarkably, μ_{orb} in pure CNs depend uniquely on their original conducting properties, length, and temperature but do not depend on the nanotube radius or the particular chirality. In doped nanotubes the magnetic moments can be strongly altered and depend on the radius and chirality. Temperature can even change their character from diamagnetic at low T to paramagnetic at high T. A general electron-hole asymmetry increasing with the doping is found.

DOI: 10.1103/PhysRevB.72.115406 PACS number(s): 73.22.−f, 75.75.+a, 73.23.Ra

I. INTRODUCTION

The electronic fate of a carbon nanotube (CN) is, in general, determined once it has been grown. Depending on the radius and the chiral angle it can be semiconducting or metallic. The electronic properties of CN can, however, be modulated by coaxial magnetic field via the Bohm-Aharonov (BA) effect, which can turn a metallic CN into a semiconducting one and vice versa. This has been predicted by Ajiki and Ando,[1] followed by Lu[2] and observed recently in three independent measurements.[3–5] CN have an ideal structure for studying the effect of the BA flux on the energy spectrum. A magnetic field B introduces a phase factor in the electron wave function in the circumferential direction and leads to a shift in the energy bands. The value of the energy shift depends on the strength of the applied field and on the orbital magnetic moment. This can be observed, e.g., as a change in the band gap structure by measuring the conductance of a single nanotube suspended between two electrodes.[3,4] The magnetic field influences the motion of electrons around the circumference of CN, giving rise to persistent currents[6,7] which at low temperatures do not decay. Persistent current multiplied by the CN cross section gives the orbital magnetic moment μ_{orb} directed along the axis.

In the present paper we investigate the dependence of $\mu_{\mathrm{orb}}(\phi,T)$ on temperature, nanotube parameters [radius (R), chirality, length], and the value of the chemical potential, which changes with doping. This is an extension of the work of Ajiki and Ando,[1] who calculated the magnetic moment μ_{orb} for an undoped tube at $T=0$.

We calculate μ_{orb} in single-wall CNs in the extended tight binding approximation (TBA with the correction resulting from the overlap between neighboring π orbitals) for various chiralities, lengths, and radii (provided that $R>10$ Å), for a range of electron- or hole-doping values. We study both isolated nanotubes, where the number of electrons $N_e=\mathrm{const}$ and nanotubes connected to a particle reservoir (e.g., as a part of a circuit), where the chemical potential $\mu_{\mathrm{chem}}=\mathrm{const}$.

We find that in undoped nanotubes the character of the magnetic moment depends only on the CN's conducting properties (i.e., whether the tube is metallic or semiconducting), its length, and the temperature of the system. On the other hand, in hole- or electron-doped nanotubes the behavior of $\mu_{\mathrm{orb}}(\phi)$ depends strongly on the chirality of the nanotube, on its size, and on the degree of hole or electron doping.

In our model calculations we study nanotubes in the ballistic regime and we work in the noninteracting electrons approximation, which has yielded good agreement with experimental results in mesoscopic rings[8] and in carbon nanotubes.[4,9,10]

II. THE MODEL

Carbon nanotubes are commonly considered and analyzed as rolled-up graphene planes. We follow here the same approach, working in the basis in which the lattice generators are $\mathbf{T}_1=\sqrt{3}e_x$, $\mathbf{T}_2=\sqrt{3}/2e_x+3/2e_y$, and the length unit is the length of the $C—C$ bond, 1.42 Å.[11,12] A nanotube is uniquely defined by four parameters $(m_1,m_2)\times(p_1,p_2)$, which define its circumference and length vectors,

$$\mathbf{L}_\perp = m_1\mathbf{T}_1 + m_2\mathbf{T}_2 \quad \text{for the circumference,}$$

$$\mathbf{L}_\parallel = p_1\mathbf{T}_1 + p_2\mathbf{T}_2 \quad \text{for the length.} \tag{1}$$

In most theoretical works on carbon nanotubes the tube under examination is considered to be infinitely long, resulting in a continuous spectrum of momenta along the CN. Since the real CNs are very long but finite, we consider $L_\parallel<\infty$. Therefore, the momentum is quantized in both directions. We chose the longitudinal boundary conditions to be cyclic,

$$\mathbf{k}\cdot\mathbf{L}_\parallel = 2\pi l_\parallel, \quad l_\parallel \in \mathbb{Z}, \tag{2}$$

where $\parallel$ stands for the direction parallel to the length of the nanotube. We found no significant differences between currents in cyclic and open longitudinal boundary conditions (see also Ref. 13).

The magnetic field is applied parallel to the axis of the CN. The Bohm Aharonov phase factor modifies the trans-

verse boundary condition (in the direction perpendicular to the magnetic field):

$$\mathbf{k}\cdot\mathbf{L}_\perp = 2\pi\left(l_\perp + \frac{\phi}{\phi_0}\right), \quad l_\perp \in \mathbb{Z}, \tag{3}$$

where $\perp$ stands for the direction parallel to the circumference of the nanotube, ϕ is the magnetic flux, and $\phi_0 = h/e$ is the quantum flux unit. The wave vector $\mathbf{k}$ can be defined either in the (k_x, k_y) or $(k_\perp, k_\parallel)$ basis. We use the second one throughout our calculations, the first only in the dispersion relation. At fields accessible in labs, only a part of the Bohm-Aharonov period ϕ_0 could be observed in nanotubes of a small diameter. However, due to the symmetry of the system, the ϕ dependence of μ_{orb} in the full ϕ_0 period can be extrapolated from its behavior in the range $(0, \phi_0/2)$. Moreover, it is now possible to obtain a single-wall nanotube of a larger radius by burning off the external shells of a multiwalled nanotube (MWNT).[14] For a CN with $R = 60$ Å, the $\phi_0/2$ flux can be obtained at $B = 18$ T, a comercially available field.

Currents running along the circumference of the CN induce in the nanotube a magnetic moment parallel to its axis. The magnetic moment of an electron close to the Fermi level can also be calculated by the following reasoning.

The energy gap between conduction and valence states close to the Fermi surface (FS) is

$$E_g^0 = \hbar v_F (k_\perp - K_i), \quad i = 1,2, \tag{4}$$

where K_i are the Fermi points where the valence and conduction bands of graphene meet. The Bohm-Aharonov effect shifts the allowed $k_\perp$ by $\delta k_\perp(\phi)$,

$$k_\perp(\phi) = k_\perp + \delta k_\perp(\phi), \quad \delta k_\perp(\phi) = \frac{\phi}{R\phi_0}, \tag{5}$$

resulting also in the energy shift ΔE[3],

$$\Delta E \simeq \left.\frac{\partial E}{\partial k_\perp}\right|_{k_F} \delta k_\perp(\phi) = \pm \frac{\hbar v_F}{R}\frac{\phi}{\phi_0} = -\vec{\mu}_{\text{orb}}^F \cdot \mathbf{B}, \tag{6}$$

where $\vec{\mu}_{\text{orb}}^F$ is the orbital magnetic moment of an electron at (or the closest to) the Fermi surface

$$\vec{\mu}_{\text{orb}}^F = \frac{Rev_F}{2}\mathbf{e}_\parallel \tag{7}$$

($\mathbf{e}_\parallel$ is the unit vector along the CN axis). This shift of the energy states results in the change of the band gap and can convert a metallic CN into a semiconducting one and vice versa. Therefore, from now on by 'metallic' and 'semiconducting' we understand CNs which display this behavior at $\phi = 0$.

The change of the band gap with the magnetic field has been investigated in three independent measurements[3–5] and in Ref. 3 helped to determine the magnitude of the orbital magnetic moment of an electron at the FS, μ_{orb}^F. A good agreement between the experimental and the theoretical values has been found.[3] Nevertheless, the magnetic response of a CN is determined by its full magnetic moment, given by

$$\mu_{\text{orb}}(\phi,T) = -\pi R^2 \frac{\partial F(\phi,T)}{\partial \phi}, \tag{8}$$

where $F(\phi,T)$ is the free energy of the CN. In other words, μ_{orb} can be written in terms of the total current $I(\phi,T)$, which runs at the cylindrical surface in the presence of the magnetic field (for detailed derivation, see Ref. 15),

$$\mu_{\text{orb}}(\phi,T) = \pi R^2 I(\phi,T) = \pi R^2 \sum_{k_\perp,k_\parallel} \frac{1}{1+\exp\{[E_{\mathbf{k}}(\phi) - \mu_{\text{chem}}(\phi)]/kT\}} I_{\mathbf{k}}(\phi). \tag{9}$$

The sum runs over the whole Brillouin zone (BZ). When $\phi \neq 0$, the currents carried by states with $\mathbf{k}$ and $-\mathbf{k}$ do not cancel out, and a net current appears. This current is persistent at low T.

The relation between μ_{orb}^F calculated and measured in Ref. 3 and $\mu_{\text{orb}}(\phi,T)$ discussed in this paper is the following. μ_{orb}^F, being the magnetic moment of an electron at (or close to) the Fermi point, is calculated in the energy range where its dispersion relation is a linear function of $\mathbf{k}$; therefore, μ_{orb}^F is independent of the flux. The total magnetic moment $\mu_{\text{orb}}(\phi,T)$ is calculated as a sum over all $\mathbf{k}$ states, thus containing terms with nonlinear dispersion relation which cause the flux dependence of the magnetic moment. Moreover, the $\mu_{\text{orb}}(\phi,T)$ calculated from Eq. (9) takes into account the temperature dependence of the energy level occupation. This effect has been neglected in the calculation of μ_{orb}^F.

Whereas the measurements of the band gap as a function of B give the information about μ_{orb}^F (which is actually the orbital moment unit, $\mu_{\text{orb}}^F = \pi R^2 I_0$, where $I_0 = ev_F/2\pi R$ is the unit of the persistent current), the full $\mu_{\text{orb}}(\phi,T)$ could be measured in other experiments which will be sensitive to it.

The currents carried by individual momentum states at $T = 0$ are

$$I_{\mathbf{k}}(\phi) = -\frac{\partial E_{\mathbf{k}}}{\partial \phi} = -\frac{\partial E_{\mathbf{k}}}{\partial k_\perp}\frac{\partial k_\perp}{\partial \phi} = -\frac{\partial E_{\mathbf{k}}}{\partial k_\perp}\frac{2\pi}{\phi_0|\mathbf{L}_\perp|}, \tag{10}$$

where the form of $E(\mathbf{k})$ depends on the approximation used. As many experiments show the electron-hole asymmetry, we use the dispersion relation based on the tight-binding approach, but which takes into account the overlap between π orbitals on adjacent carbon atoms in the lattice.[12]

$$E_{\mathbf{k}(\phi)} = \frac{\epsilon_{2p} \pm \gamma w_{\mathbf{k}(\phi)}}{1 \mp s w_{\mathbf{k}(\phi)}}, \tag{11}$$

where

$$w_{\mathbf{k}(\phi)} = \sqrt{1 + 4\cos^2\left[\frac{\sqrt{3}}{2}k_x(\phi)\right] + 4\cos\left[\frac{\sqrt{3}}{2}k_x(\phi)\right]\cos\left[\frac{3}{2}k_y(\phi)\right]}, \tag{12}$$

ϵ_{2p} is the on-site energy, s is the overlap between the π orbitals on adjacent sites, and γ is the hopping integral for graphene. Henceforth we shall refer to this model as extended tight-binding (TBA). Various authors assume different values for γ, ranging from 2.5 to 3 eV.[4,16] Following Ref. 12 we set $\epsilon_{2p}=0$ and $s=0.129$, which is the experimentally fitted value for graphite. Magnetic flux enters the dispersion relation (11) as it modifies the wave vector $\mathbf{k}$ according to Eq. (3). The states $\mathbf{k}$ and $-\mathbf{k}$ change into $\mathbf{k}+\phi/\phi_0$ and $-(\mathbf{k}-\phi/\phi_0)$, which are not equivalent. Thus the currents carried by $\pm\mathbf{k}(\phi)$ do not cancel out and a net current appears.

The dispersion relation in the neighborhood of the Fermi points is very similar to the simple tight-binding model with $s=0$. Hence, if the physical phenomena under consideration involve only states close to $E=0$, the tight binding model is adequate. However, the persistent current comes from the contributions of all states under the Fermi level.

Additional modification in dispersion relation for nanotubes can arise from the hybridization of σ and π orbitals due to the curvature of the tube. This correction decreases with increasing radius of the CN.[12,17] For nanotubes with radius $R \approx 7$ Å a good agreement was found between experiment and π-only calculations.[12,18] As we consider CNs with relatively large radii ($R > 10$ Å), we neglect it in our model calculations.

The individual currents $I_{\mathbf{k}}(\phi)$ in Eq. (10) depend on the position of the $\mathbf{k}$ states in the Brillouin zone. The level of μ_{chem} defines the Fermi surface and determines the range of states whose contributions dominate the sum (9). The distribution of allowed momentum states in the BZ depends on the chirality of the CN. Therefore, at shifted μ_{chem}, different states fall into the dominating range depending on the chirality of the nanotube. Consequently the total magnetic moment depends on the doping level and on the chirality of the CN. At the half-filling, corresponding to undoped nanotube, the chemical potential is 0 ($\mu_{\text{chem}}=0$). Doped systems (either doped with electrons or with holes) can be studied under two different physical conditions.

If the system is connected with a particle reservoir, its chemical potential at a given doping is constant (μ_{chem} =const). The distribution of allowed momentum states in the BZ shifts with the magnetic flux, which induces a shift of the Fermi level. But the chemical potential is determined externally and the CN can absorb the number of electrons or holes necessary to keep it stable. The number of electrons then varies with the magnetic flux, $N_e=N_e(\phi)$. When the nanotube is isolated, there is no exchange of electrons with a reservoir, their number is constant (N_e=const), and the chemical potential is a function of the magnetic flux [$\mu_{\text{chem}}=\mu_{\text{chem}}(\phi)$]. The magnetic moments have different shapes in isolated than in connected nanotubes. We performed the calculations in both cases.

We have calculated numerically the magnetic moment according to Eq. (9). In the case of a constant number of electrons, the chemical potential has been found at each value of ϕ from the condition $\Sigma_{(k_\perp,k_\parallel)} f_{\text{FD}}[E_{(k_\perp,k_\parallel)}(\phi)]=N_e$, where $f_{\text{FD}}[E_{\mathbf{k}}(\phi)]$ is the Fermi-Dirac distribution function.

III. ORBITAL MAGNETIC MOMENTS—UNDOPED NANOTUBES

Several effects concerning the persistent currents and induced magnetic moments in a parallel magnetic field can be deduced from an analysis of the structure of the energy spectrum and the Brillouin zone. In this section we discuss undoped nanotubes, i.e., $\mu_{\text{chem}}=0$ and the number of electrons is equal to the number of nanotube lattice sites, i.e., $N_e = m_1 p_2 - p_1 m_2$. In this case there is no difference between the μ_{chem}=const and N_e=const conditions. The number of states below the Fermi level is the same as in the Brillouin zone, consequently, N_e=const regardless of the value of the external magnetic flux. The energy gap opens or closes with changing ϕ, but the chemical potential is fixed at 0.

A. $\mu_{\text{orb}}(\phi,T)$ in metallic and semiconducting CNs

There are two types of behavior of $\mu_{\text{orb}}(\phi,T)$. In metallic nanotubes it is paramagnetic at $\phi=0$, whereas in semiconducting ones it is diamagnetic. It is shown in Fig. 1 for $T=0$ and $T=300$ K. The characteristic shape of the curves for metallic (M) and semiconducting (S) nanotubes has been obtained by Ajiki and Ando[1] in $\mathbf{k}\cdot\mathbf{p}$ approximation and for zigzag nanotubes in the tight binding approximation at $T=0$. Our calculations have been performed in extended TBA and $T\neq 0$ for armchair, zigzag, and chiral nanotubes, and show that this effect does not depend on the particular chirality of the metallic or semiconducting nanotube.

It is so because the main component of the magnetic moment (9) comes from the $\mathbf{k}$ states close to the Fermi points $\mathbf{K}_i$. The dispersion relation in the neighborhood of these points has a form of two cones and therefore rotational symmetry.[19] Because of that, $\partial E/\partial k_\perp$ is independent of the particular angle (determined by m_1 and m_2) at which $k_\perp$ =const lines (see Fig. 2) lie with respect to the edges of the Brillouin zone. In the case of metallic CNs, these momentum lines cross the Fermi points and the magnetic moment has the M shape from Fig. 1. Due to the peculiar band structure of the CNs, the magnetic moment in a semiconducting CN (s) has an unusual shape, with a plateau around $\phi_0/2$. Close inspection of the structure of momentum lines in the BZ shows that it is a superposition of two metallic moments, shifted by $\pm\phi_0/3$ (as shown in Fig. 3). They are generated by the two momentum ($k_\perp$=const) lines which reach the Fermi point, one at $\phi=-\phi_0/3$ and the other at $+\phi_0/3$, indepen-

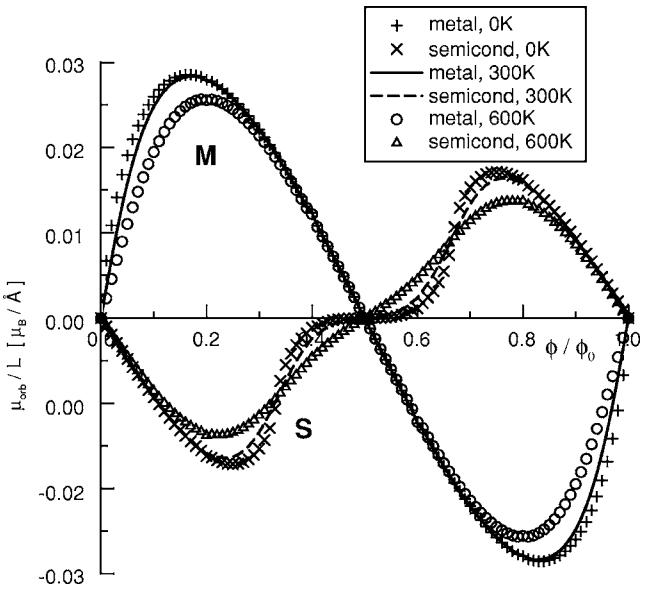

FIG. 1. Orbital magnetic moment per Å in a single-wall nanotube of radius 25 Å, for different chiralities. All metallic nanotubes have the same (up to 1%) $\mu_{\mathrm{orb}}(\phi)$. The same is true for the semiconducting nanotubes. The change of the magnetic moments between $T=0$ K and $T=300$ K is very small.

dently of chirality. The amplitude of this sum is then smaller than in the metallic CN, where both momentum lines reach the Fermi points at the same ϕ. The slope of μ_{orb} vs ϕ (see Fig. 1) is steeper for these values of ϕ where the CN is metallic, since the paramagnetic behavior of the μ_{orb} is

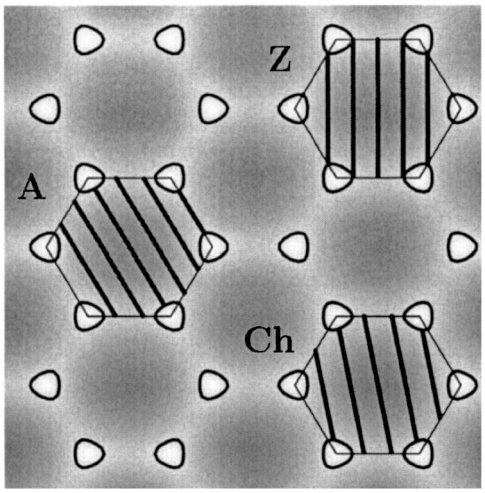

FIG. 2. The reciprocal lattice of graphene, with momentum states and first Brillouin zones of Zigzag (5,0), Armchair (3,3), and Chiral (4,1) nanotubes doped to -0.6γ. The Fermi contours are the thick triangular loops and the thick straight lines correspond to $k_\perp$ =const lines. In undoped nanotubes all momentum states in the Brillouin zone enter into the sum from Eq. (9) and $\mu_{\mathrm{orb}}(\phi)$ is chirality independent. In doped nanotubes only those states which lie below the Fermi level (outside the loops) contribute to the sum. Note that the number of missing states (the missing fragments of $k_\perp$=const lines) is different in A, Z, and Ch cases, which results in the chirality dependence of $\mu_{\mathrm{orb}}(\phi)$.

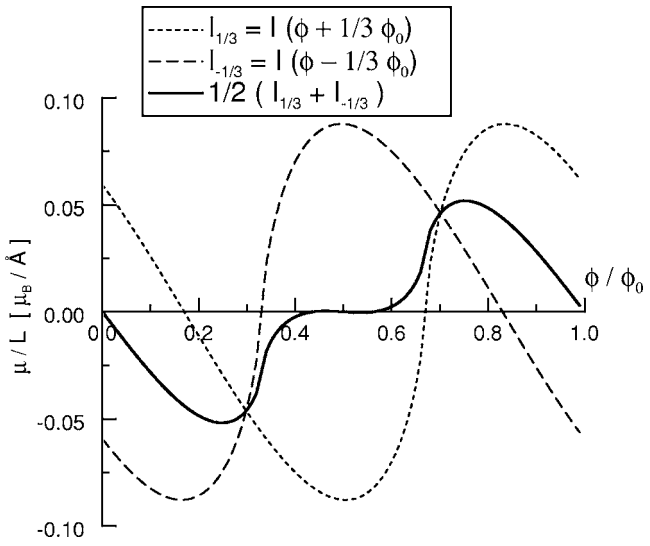

FIG. 3. The magnetic moment per Å in a semiconducting nanotube as a superposition of two metallic moments shifted by $\pm\phi_0/3$.

caused by momentum states crossing the Fermi surface, whose contributions to the magnetic moment are the most significant. On the contrary, the gentle slope of μ_{orb} in the semiconducting regime is caused by the diamagnetism of the states below the FS. Thus the inspection of the slope of $\mu_{\mathrm{orb}}(\phi)$ can help to observe an extraordinary feature of CNs, namely that they can be converted from metallic to semiconducting and vice versa by the application of a magnetic field.

B. Temperature dependence

The magnitude of the orbital magnetic moment, contrary to the spin magnetic moment, decreases with temperature although this decrease is not very dramatic for the ranges of magnetic field accessible in labs. It is more important for CN with larger R, since the energy gap scales like $1/R^2$. In con-

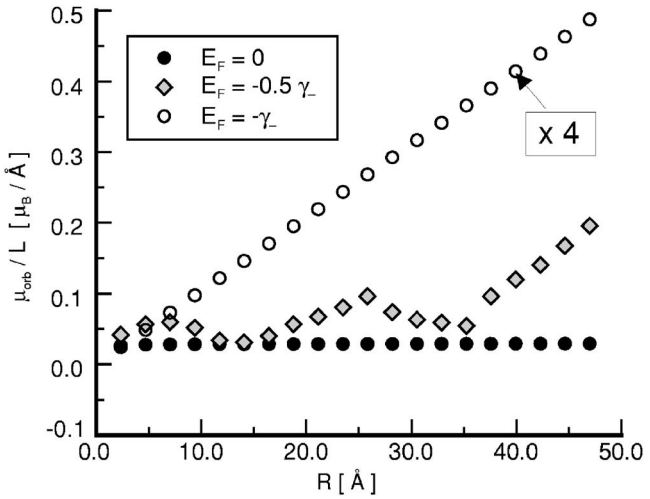

FIG. 4. The dependence of the magnetic moment per unit length on the nanotube radius in zigzag nanotubes ranging from (6, 0) to (120, 0), at half-filling and at two values of doping. The magnetic moment at $E_F=-\gamma_-$ is divided by 4 so as to fit in the plot.

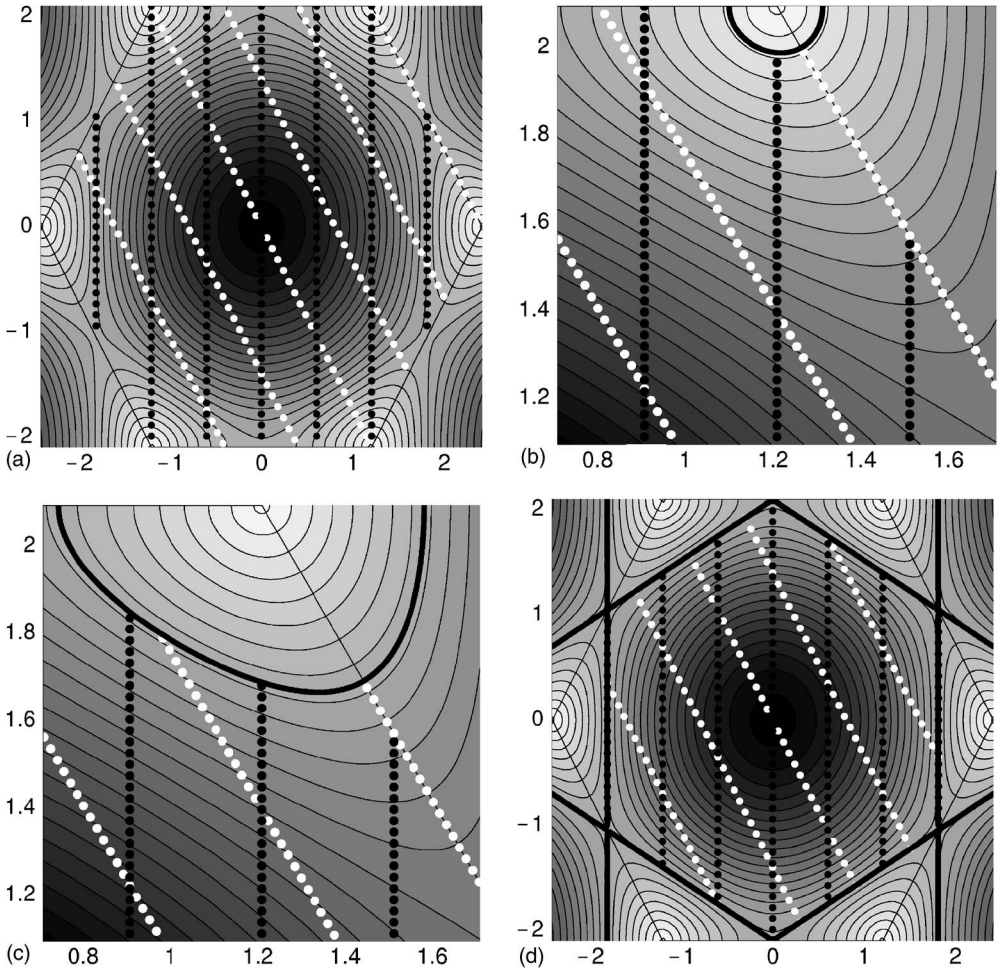

FIG. 5. The Brillouin zone and momentum states of an arbitrary armchair (white dots) and zigzag (black dots) nanotube of similar radius, at $\phi=0$. The background is the contour plot of $E_{\mathbf{k}}$ from Eq. (11). The Fermi contour is marked by thick solid lines. (a) Full Brillouin zone, undoped nanotube ($\mu_{\text{chem}}=0$). The Fermi surface reduces to two points at the vertices of the hexagon. (b) The neighborhood of the Fermi point $(2\pi/(3\sqrt{3}),2\pi/3)$, $\mu_{\text{chem}}=-0.16\gamma$. The contour is circular and both nanotubes respond with almost the same magnetic moments (see Fig. 7), momentum lines cross the Fermi contour at identical angles. (c) The neighborhood of the Fermi point $(2\pi/(3\sqrt{3}),2\pi/3)$, $\mu_{\text{chem}}=-0.6\gamma$. The Fermi contour loses the rotational symmetry and magnetic moments in zigzag and armchair nanotubes differ (see Fig. 10). (d) Full Brillouin zone, $\mu_{\text{chem}}=-\gamma$. The Fermi contour is a closed hexagon, with two sides parallel to the momentum lines in the zigzag nanotube. Currents in this tube are very strongly enhanced (cf. Fig. 9), in others suppressed (cf. Fig. 8).

sequence, for example, in multiwall CN, the measurements should be performed at lower T. Since the main effect of temperature on $\mu_{\text{orb}}(\phi,T)$ in undoped nanotubes is a small suppression of its amplitude (cf. Fig. 1), we shall in this section assume $T=0$ and analyze only $\mu_{\text{orb}}(\phi,0)$, which we shall denote by $\mu_{\text{orb}}(\phi)$.

When the distance between momentum lines $\Delta k_\perp$ becomes small enough (i.e., when $R>10$ Å), $I_{\mathbf{k}}(\phi,T)$ is linear in $\Delta k_\perp$ and two effects appear.

C. Length scaling of the magnetic orbital moments

The sum of $I(\mathbf{k})$ grows linearly with the number of states on one momentum ($k_\perp=$const) line, which is proportional to the length of the nanotube. This is also true for doped nanotubes.

D. Independence of $\mu_{\text{orb}}(\phi)$ of the nanotube radius

The radius of the nanotube affects $\mu_{\text{orb}}(\phi)$ in two ways: (i) The cross section of a nanotube $\sim R^2$, and (ii) From Eq. (10) we conclude that the current of an individual $\mathbf{k}$ state $\sim 1/R$ because $\partial E_{\mathbf{k}}/\partial k_\perp$ is constant for a given $\mathbf{k}$. The summation over the whole Brillouin zone in Eq. (9) yields another $1/R$ factor and as a result the whole sum is proportional to $1/R^2$. These two effects lead to $\mu_{\text{orb}}(\phi)$ nearly independent of R (see black circles in Fig. 4), in agreement with Ref. 1. This result in undoped CNs does not depend on the chirality of the nanotube. Note that $\mu^F_{\text{orb}}(\phi)$ calculated and measured in Ref. 3 increases linearly with R because it is due only to electrons closest to the Fermi level.

Thus for any undoped metallic or semiconducting nanotube the total magnetic moment depends only on its length and on temperature, and has either the M (in metallic CNs) or the S (in semiconducting CNs) form from Fig. 1.

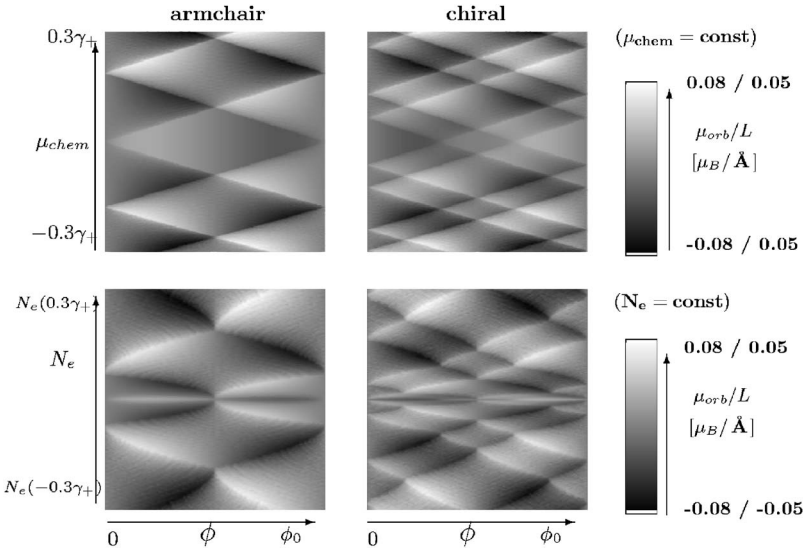

FIG. 6. The comparison between (top) $\mu_{\rm chem}$ =const and (bottom) N_e=const conditions on the conical part of the dispersion relation, i.e., for $|\mu_{\rm chem}| \leqslant 0.3\gamma_+$. The left column shows the orbital magnetic moment per Å (color scale) in armchair (15,15); the right column shows chiral semiconducting (15,14) nanotubes.

IV. ORBITAL MAGNETIC MOMENTS—DOPED NANOTUBES

The peculiar band structure of graphene is reflected in the variety of behaviors of CNs with different chiralities upon doping. We performed the calculations of the full magnetic moment $\mu_{\rm orb}(\phi,T)$ for zigzag, armchair, and chiral nanotubes. We found that it depends significantly on doping; being the sum of the terms below the FS, it depends strongly on the shape of the FS which changes with the number of holes or electrons introduced in the system.

A. Isolated or connected: $\mu_{\rm chem}$=const versus N_e=const approach

Different results were obtained for $\mu_{\rm chem}$=const (nanotube in a circuit) and N_e=const (isolated nanotube). Both conditions can be realized experimentally. The calculations were performed for both electron and hole doping, changing the Fermi level from E_F=0 (no doping) to $E_F = \pm\gamma_\pm$. $\gamma_\pm = \gamma/(1 \mp s)$ denotes the value of energy in, correspondingly, the conduction (+) and valence (−) band, at the centers of the edges of the Brillouin zone. In the case of nanotubes doped to $E_F = \pm\gamma_\pm$ we found that again there is no difference between N_e=const and $\mu_{\rm chem}$=const, because the Fermi contour has then the hexagonal symmetry of the Brillouin zone [cf. Fig. 5(d)] and the number of momentum states within it is constant with ϕ. At intermediate doping the two approaches give distinctly different results, which are shown in Fig. 6. Note, for instance, that in an isolated nanotube (N_e =const) the magnetic moment at half-filling (the central area of the bottom row plots in Fig. 6) changes completely when even a few electrons are added or removed from the system. At constant chemical potential the dependence of $\mu_{\rm orb}(\phi,T)$ on doping is more smooth.

All results discussed in the following sections are valid in both cases, without qualitative differences. Therefore we present in detail only the results for $\mu_{\rm chem}$=const.

B. Dependence of $\mu_{\rm orb}(\phi)$ on the nanotube radius

The independence of $\mu(\phi,T)$ on the radius of the nanotube shown in Fig. 4 is characteristic for undoped nanotubes

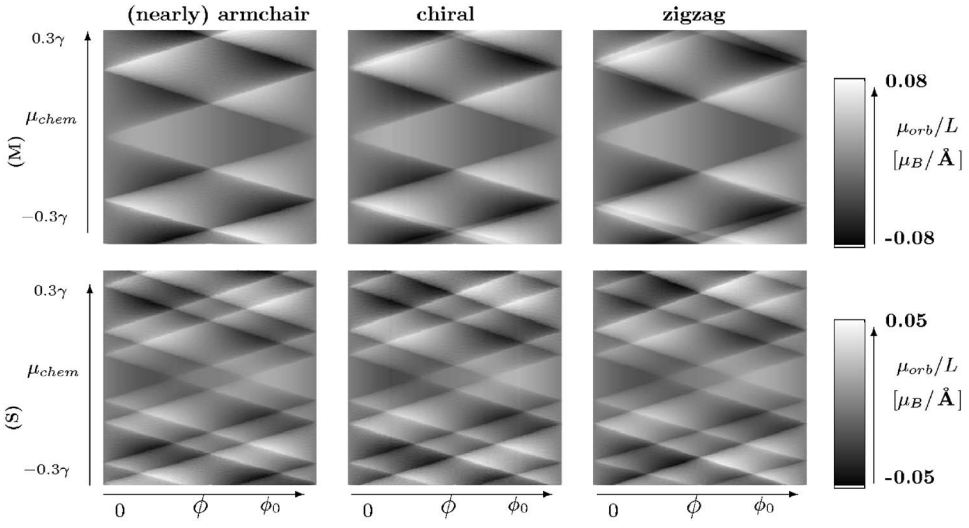

FIG. 7. The orbital magnetic moment per unit length (gray-scale) for $|\mu_{\rm chem}| \leqslant 0.3\gamma$, for metallic (top row) armchair (15,15), chiral (19,10), and zigzag (24,0) nanotubes, and for semiconducting (bottom row) nanotubes with similar chiralities: (15,14), (19,9), and (25,0). R=10.2 Å, T=0. The Fermi contour around a Fermi point in this regime is almost circular, which accounts for the similarities between the three cases.

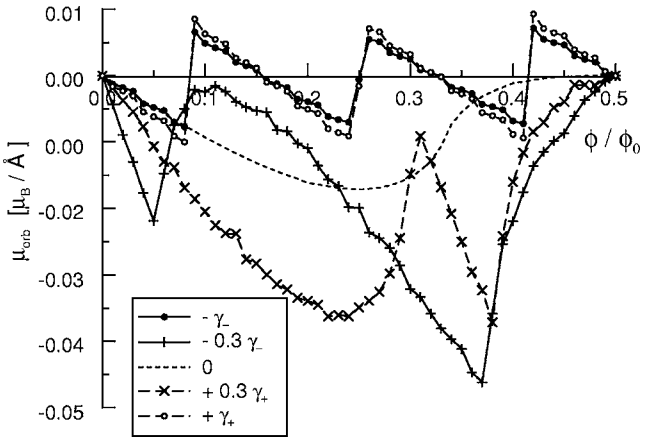

FIG. 8. The magnetic moment per unit length in a nearly armchair $(38,36)\times(-4028,4101)(R=25$ Å) nanotube. $E_F=0$, $\pm 0.3\gamma_\pm$, $\pm\gamma_\pm$, for $\mu_{\text{chem}}=$const, at $T=0$ K.

only. The sum in Eq. (9) is in that case over the whole Brillouin zone and the dominating currents come from the momentum states in the neighborhood of the Fermi points $\mathbf{K}_i$, where the dispersion relation is conical. On the other hand, if the doping reaches the value $E_F=\pm\gamma_\pm$, the amplitude of $\mu_{\text{orb}}(\phi,T)$ grows linearly with the radius of the nanotube (for an illustration of a hole-doped zigzag case, see Fig. 4). The currents dominating the sum are those from the states near the Fermi contour, which in this case is the inner hexagon in Fig. 5(d); the dispersion relation below $-\gamma_-$ is nearly parabolic. As we lower the chemical potential of the nanotube, we cross from the regime of the magnetic moment independent of R (conical dispersion relation near $E_F=0$) to the regime where it depends linearly on R (quasiparabolic near $E_F=-\gamma_-$). The Brillouin zone in the intermediate regime is shown in Figs. 2, 5(b), and 5(c). The magnetic moment depends then on the nanotube radius in a more complicated way (an example is shown in Fig. 4 as gray diamonds). Note that the linear dependence of the magnetic moments on the radius in the case of $E_F=-\gamma_-$ resembles that of persistent currents in metallic cylinders.[20,21]

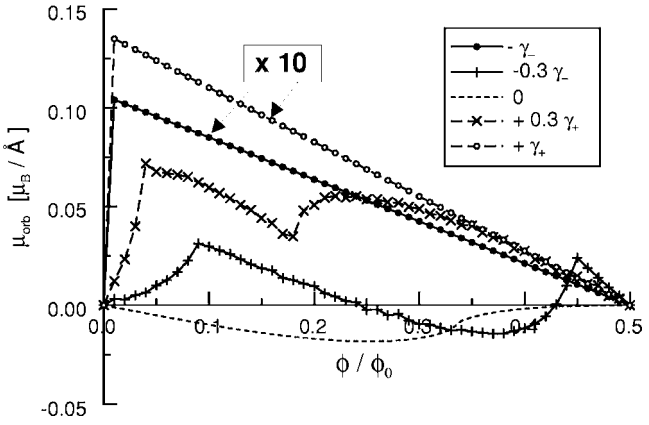

FIG. 9. The magnetic moment per unit length in a zigzag $(64,0)\times(-2347,4694)(R=25$ Å) nanotube, at $E_F=0$, $\pm 0.3\gamma_\pm$, $\pm\gamma_\pm$, both for $\mu_{\text{chem}}=$const, at $T=0$ K. The magnetic moment at $\mu_{\text{chem}}=\pm\gamma_\pm$ is divided by 10 so as to fit into the plot.

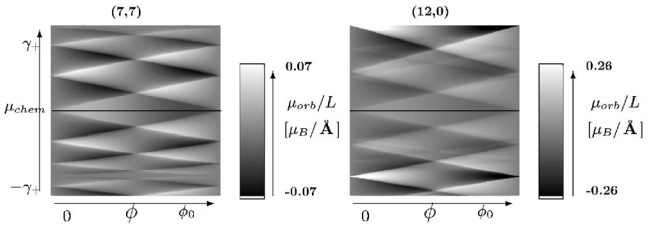

FIG. 10. The magnetic moment per unit length (grayscale) in (7,7) armchair (left) and (12,0) metallic zigzag (right) hole-doped nanotubes ($R\approx 5.2$ Å). The range of chemical potential is from $-\gamma_+$ to γ_+. The part corresponding to an electron-doped nanotube is not symmetrical to the hole doped. At a chemical potential lower than $\sim -0.3\gamma$ (lower part of the plots), the Fermi contour ceases to be circular and the μ_{orb} patterns become different for different chiralities. The straight line marks $\mu_{\text{chem}}=0$.

C. Symmetry properties of $\mu_{\text{orb}}(\phi,T)$ under electron and hole doping

In case of a symmetric dispersion relation with $s=0$, the $\mu_{\text{orb}}(\phi,T)$ is identical under electron and hole doping. It is a combined effect of the symmetry of the Fermi-Dirac function with respect to the chemical potential, and the hole-electron symmetry of the dispersion relation of graphene which both enter Eq. (9). If, however, the dispersion relation is asymmetric ($s\neq 0$), the orbital magnetic moments show only an approximate symmetry for very small doping (see Figs. 6 and 7). At higher values of doping we find considerable asymmetry of μ_{orb} between hole and electron doping. It is shown in Figs. 8–10.

In a recent experiment[22] an electron-hole symmetry was found in differential conductance measurements for a semiconducting nanotube. The orbital moment in a semiconducting nanotube also shows this symmetry at small ϕ and small doping, which are the conditions in the experiment mentioned above. The authors of the experiment investigated the range of 20 excess holes or electrons. We find that for a doping larger than to $\approx$35 electrons or holes and nanotubes of the size used in Ref. 22, an asymmetry should appear even in very clean tubes. An experimental study of a wider range of doping might help to determine the actual value of s in CNs.

D. Dependence of $\mu_{\text{orb}}(\phi,T)$ on the chirality of the nanotube

The shape of the Fermi contour in a CN changes significantly with doping,[23] from two points [Fig. 5(a)], through a set of increasingly flattened circles [Figs. 5(b) and 5(c)], to a hexagon [Fig. 5(d)]. That is why in doped nanotubes the form of the magnetic moment as a function of magnetic field and temperature depends strongly on the chirality of the nanotube and reflects the geometrical relation of their momentum lines to the actual shape of the Fermi surface (see Figs. 5, 8, and 9). The paramagnetic contribution to the persistent current and consequently to the magnetic moment is enhanced if the number of states crossing the Fermi level simultaneously is large; therefore, the strongest magnetic response should be achieved in systems with momentum lines nearly parallel to the Fermi surface.[23] This is achieved in a

TABLE I. Magnetic orbital moment at μ_{chem}=const for SWNT of radius 25 Å, length 0.1 μm, for various chiralities and levels of electron or hole doping μ_{chem}. The unit is μ_B, values in brackets (italics) are for electron doping, outside brackets for hole doping. The orbital moments greater than $100\mu_B$ are in bold font. The values in the table are the maximum values obtainable in magnetic fields ranging from 0 to 20 *T*.

μ_{chem}	0	$-0.3\gamma_-(+0.3\gamma_+)$	$-0.6\gamma_-(+0.6\gamma_+)$	$-\gamma_-(+\gamma_+)$
armchair (37,37)	26	5.1 *(48)*	46 ***(122)***	$\leqslant$1 *($\leqslant$1)*
chiral S (38,36)	−9	−26 *(−20)*	−39 *(−35)*	−8 *(9)*
chiral M (48,24)	26	19 *(23)*	−34 *(−25)*	−3 *(−4)*
chiral S (49,23)	−9	−46 *(−21)*	−23 *(37)*	$\leqslant$1 *($\leqslant$1)*
chiral S (63,2)	−9.7	29 *(59)*	−49 *(12)*	**117** ***(151)***
zigzag M (63,0)	26	67 *(19)*	37 *(−96)*	**−210** ***(−270)***
zigzag S (64,0)	−9.8	−29.6 *(59.6)*	−49 *(16)*	**1060** (***1370***), at $B \ll 1$T

zigzag CN doped to such a value of E_F that the FS becomes a hexagon. This doping is $\gamma_- \approx 0.89\gamma$ for holes and $\gamma_+ \approx 1.15\gamma$ for electrons. The lines of states [marked by black dots in Fig. 5(d)] are then parallel to two sides of the Fermi surface (inner hexagon). The resulting magnetic moment is huge—see Fig. 9 and Table I.

E. Temperature dependence of $\mu_{\text{orb}}(\phi,T)$

The main effects of temperature on $\mu_{\text{orb}}(\phi,T)$ are a suppression of its amplitude and its smoothing into a sinusoidal shape. The latter effect smoothes out all sharp features in the $\mu_{\text{orb}}(\phi,T)$ dependence (absent in undoped nanotubes) and can even turn a diamagnetic moment at $T=0$ into a paramagnetic one at $T=300$ K (see Fig. 11).

F. Dependence of $\mu_{\text{orb}}(\phi)$ on the value of doping

This dependence shows several interesting features (see Figs. 7 and 10).

First, as long as the doping does not exceed $\pm 0.3\gamma$, the orbital magnetic moments fall in two distinct classes, depending on whether the nanotube was originally metallic or semiconducting. This feature is due to the fact that the Fermi surface for small dopings is a set of nearly circular loops, meeting at the same angle the momentum lines of any chirality [cf. Figs. 5(b) and 7].

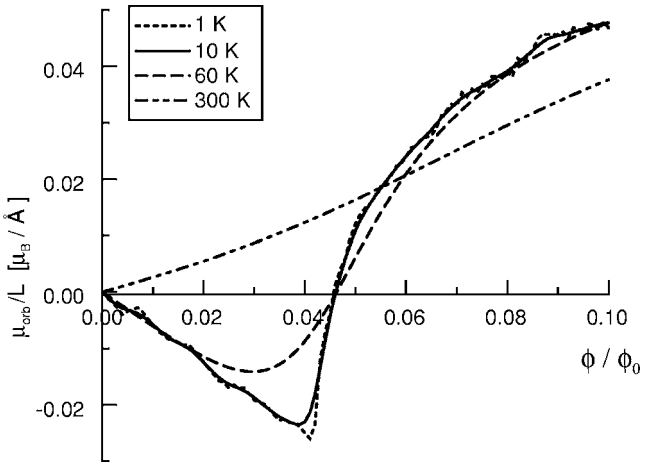

FIG. 11. The magnetic moment per unit length in a nearly armchair $(38,36)\times(-4028,4101)$. The doping is fixed at $0.3\gamma_+$. The temperature changes the character of μ_{orb} from diamagnetic (small *T*) to paramagnetic (high *T*).

As the Fermi surface loses the circular symmetry at larger values of doping, differences appear between nanotubes of the same type of conduction and different chiralities [cf. Figs. 5(c) and 10]. The doping level at which the maximum amplitude of the magnetic moments is reached depends on the chirality of the CN.

The sawtooth shape of the orbital magnetic moment in a $(38,36)\times(-4028,4101)$ nanotube doped to $\pm\gamma_\pm$ in Fig. 8 is a manifestation of the fractional period of the Bohm-Aharonov effect, noticed by Sasaki *et al.*[24] In CNs whose length is commensurate with their circumference, the period of the Bohm-Aharonov oscillations is a fraction of ϕ_0.

V. CONCLUSIONS

CNs can be one of the basic ingredients of the future nanoelectronic devices. Therefore their behavior in the magnetic field is of big importance. The magnetic field has a strong effect on the electronic structure of the CN: it can be used to tune the energy spectrum. This raises the possibility of controlling the energy levels through an external field, opening the door to further studies of fundamental properties of nanotubes as well as technological applications. When applied parallel to the tube axis, the magnetic field creates orbital magnetic moments, which depend strongly on the chirality, length, and doping level of the CN.

The results of our model calculations show that the behavior of the orbital magnetic moment in single-wall nanotubes has the following features: (i) the temperature diminishes its amplitude and smoothes out sharp features in the $\mu_{\text{orb}}(\phi,T)$ dependence, which in doped nanotubes can even change the character of the response from diamagnetic at low *T* to paramagnetic at high *T* (cf. Fig. 11); (ii) its dependence on ϕ is very similar in electron- and hole-doped CNs, at small values of doping, in nanotubes both isolated and forming part of a circuit. At larger values of doping the asymmetry becomes significant; (iii) is nearly independent of *R* in half-filled CNs and depends on *R* in the doped ones; in case

of $E_F=-\gamma_-$ this dependence is linear; (iv) scales with length in both pure and doped CNs; (v) is independent of chirality for pure CNs and depends strongly on chirality in heavily doped nanotubes. In this paper we have given a survey of the properties of the orbital magnetic moments for single-wall nanotubes of different chiralities with different radii and length, and for various values of electron or hole doping, at zero and finite temperatures. In multiwall nanotubes these dependences are more complex, since all shells are penetrated by the magnetic field and all must be taken into account. The magnetic moments are then a superposition of moments from different shells. Some aspects of this problem have recently been discussed in Refs. 15,25.

The magnetization and susceptibility of multiwall carbon nanotubes and nanotori has been the subject of both theoretical and experimental study.[26,27] These measurements were performed with a SQUID device.

It seems that the measurement of the orbital magnetic moment may also be possible, e.g., in a setup with a double-walled CN. The outer shell can be used as a field detector. The current running along it would be modified by the Bohm-Aharonov effect. The precise measurement of this current, compared with the current in identical but single-walled CN, could reveal the magnetic moment produced by the inner tube.

ACKNOWLEDGMENTS

This work was supported by the Polish Ministry of Scientific Research and Information Technology under Grant No. PBZ-MIN-008/P03/2003 M.S. thanks Hélène Bouchiat for valuable discussions.

*Corresponding author. Email address: magda@phys.us.edu.pl

[1] H. Ajiki and T. Ando, J. Phys. Soc. Jpn. **62**, 2470 (1993).
[2] J. P. Lu, Phys. Rev. Lett. **74**, 1123 (1995).
[3] E. D. Minot, Y. Yaish, V. Sazonova, and P. McEuen, Nature **428**, 536 (2004).
[4] U. C. Coskun, T.-C. Wei, S. Vishveshwara, P. M. Goldbart, and A. Bezryadin, Science **304**, 1132 (2004).
[5] S. Zaric, G. N. Ostojic, J. Kono, J. Shaver, V. C. Moore, M. S. Strano, R. H. Hauge, R. E. Smalley, and X. Wei, Science **304**, 1129 (2004).
[6] M. Büttiker, Y. Imry, and R. Landauer, Phys. Lett. **96**, 365 (1983).
[7] H.-F. Cheung, Y. Gefen, E. K. Riedel, and W.-H. Shih, Phys. Rev. B **37**, 6050 (1988).
[8] B. Reulet, M. Ramin, H. Bouchiat, and D. Mailly, Phys. Rev. Lett. **75**, 124 (1995).
[9] T. W. Odom, J.-L. Huang, P. Kim, and C. M. Lieber, J. Phys. Chem. B **104**, 2974 (2000).
[10] S. Latil, S. Roche, and A. Rubio, Phys. Rev. B **67**, 165420 (2003).
[11] J. Gonzalez, F. Guinea, and M. A. H. Vozmediano, Int. J. Mod. Phys. B **112**, 4331 (1993).
[12] R. Saito, G. Dresselhaus, and M. S. Dresselhaus, *Physical Properties of Carbon Nanotubes* (Imperial College Press, London, 1998).
[13] F. Bloch and H. Rorschach, Phys. Rev. **128**, 1697 (1962).
[14] P. G. Collins, M. S. Arnold, and Ph. Avouris, Science **292**, 706 (2001).
[15] M. Margańska, M. Szopa, and E. Zipper, Acta Phys. Pol. A **106**, 609 (2004).
[16] M. F. Lin and D. S. Chuu, Phys. Rev. B **57**, 6731 (1998).
[17] X. Blase, L. X. Benedict, E. L. Shirley, and S. G. Louie, Phys. Rev. Lett. **72**, 1878 (1994).
[18] P. Kim, T. W. Odom, J.-L. Huang, and C. M. Lieber, Phys. Rev. Lett. **82**, 1225 (1999).
[19] P. L. McEuen, M. Bockrath, D. H. Cobden, Y.-G. Yoon, and S. G. Louie, Phys. Rev. Lett. **83**, 5098 (1999).
[20] H. Cheung, Y. Gefen, and E. K. Riedel, IBM J. Res. Dev. **32**, 359 (1988).
[21] M. Stebelski, M. Szopa, and E. Zipper, Z. Phys. B: Condens. Matter **103**, 79 (1997).
[22] P. Jarillo-Herrero, S. Sapmaz, C. Dekker, L. P. Kouwenhoven, and H. S. J. van der Zant, Nature **429**, 389 (2004).
[23] M. Szopa, M. Margańska, and E. Zipper, Phys. Lett. A **299**, 593 (2002).
[24] K. Sasaki, S. Murakami, and R. Saito, Phys. Rev. B **70**, 233406 (2004).
[25] M. Szopa, M. Margańska, E. Zipper, and M. Lisowski, Phys. Rev. B **70**, 075406 (2004).
[26] V. Likodimos, S. Glenis, N. Guskos, and C. L. Lin, Phys. Rev. B **68**, 045417 (2003).
[27] C. C. Tsai, F. L. Shyu, C. W. Chiu, C. P. Chang, R. B. Chen, and M. F. Lin, Phys. Rev. B **70**, 075411 (2004).